

Article

# Modelling of the Dynamic Young's Modulus of a Sedimentary Rock Subjected to Nonstationary Loading

Mikhail Guzev <sup>1,2</sup>, Evgenii Riabokon <sup>1,\*</sup>, Mikhail Turbakov <sup>1</sup>,  
Evgenii Kozhevnikov <sup>1</sup> and Vladimir Poplygin <sup>1</sup>

<sup>1</sup> Department of Oil and Gas Technologies, Perm National Research Polytechnic University, 614990 Perm, Russia; guzev@iam.dvo.ru (M.G.); msturbakov@gmail.com (M.T.); kozhevnikov\_evg@mail.ru (E.K.); poplygin@bk.ru (V.P.)

<sup>2</sup> Institute of Applied Mathematics, Far Eastern Branch of the Russian Academy of Sciences, 690041 Vladivostok, Russia

\* Correspondence: riabokon.evgenii@gmail.com

Received: 27 October 2020; Accepted: 3 December 2020; Published: 7 December 2020



**Abstract:** This paper presents a mathematical model that reflects the nature of the dynamic Young's modulus of a dry sedimentary rock during nonstationary uniaxial loading. The model is based on an idealized model of a system suggested by Jaeger J.C. A rock sample is considered as a spring with stiffness, the bottom point of which is fixed, while the upper point carries a mass. A sample experiences dynamic load and the rock matrix response. Displacement of the mass from the equilibrium state sets the variation of the sample's length. Displacement of all the sample's points goes according to the same law regardless of the point location. The response of a rock to a disturbing nonstationary load is selected based on the combination of conditions of each experiment, such as the load frequency and amplitude and the mass, length, and diameter of a sample. The mathematical model is consistent with experimental data, according to which an increase in load frequency leads to an increase in the dynamic Young's modulus for each value of the load. The accuracy of the models is evaluated. The relations underlying the model can be used as a basis to describe the Young's modulus dispersion of sedimentary rocks under the influence of nonstationary loads.

**Keywords:** dynamic load; elasticity; mathematical model; sandstone; experimental data

## 1. Introduction

The elastic characteristics of sedimentary rocks change under the influence of nonstationary loads (e.g., vibrations) [1–3]. Consideration of the change of elastic characteristics under dynamic loads is essential during geomechanical modelling. The accuracy of geomechanical modelling, as well as the reliability of constructed geotechnical structures, depends on the values of elastic characteristics [4], the dynamic Young's modulus in particular, and phenomena laid out in the model. The most common technique for estimation of the dynamic Young's modulus of sedimentary rocks is the elastic wave theory, which is grounded in the principles of acoustic wave propagation through a porous rock [5–15]. According to such an approach, the dynamic Young's modulus is estimated using the velocity of waves, elastic constants, and rock density [16]. The other techniques, such as that used in [17], are based on dynamic uniaxial loading (sinusoidal cyclic compression) and consider the dependence of the dynamic component of the Young's modulus as an approximation function of the frequency  $\omega$  and amplitude  $A$  of a periodic load. The techniques based on a hysteresis loop during cyclic loading [18,19] allow us to calculate the dynamic Young's modulus using the conventional formulas given in [20]. Despite the fact that the existing techniques are able to calculate the dynamic component of the Young's modulus

in certain conditions, they do not provide us with any model or physically substantiated relations of a nonlinear nature of the dynamic Young's modulus depending on the nonstationary load frequency, amplitude, and physical parameters of the studied rock. Therefore, the purpose of this paper is to produce a model based on physically substantiated relations that would determine the nonlinear behavior of the dynamic component of the Young's modulus under the influence of a nonstationary load with a given frequency and amplitude. Such relations allow us to differentiate the origin of the nonlinear behavior of the dynamic Young's modulus, calculate its value, and subsequently use it in geomechanical modelling.

The paper is organized as follows. In Section 2, details of the previously conducted experimental study are presented to describe the methodology of the Young's modulus determination. Then, a model of the sedimentary rock dynamic Young's modulus, including a set of parameters, is formulated in Section 3, followed by results and discussion in Section 4. Finally, the conclusions of this study are presented in Section 5.

## 2. Description of the Experiment

A medium-grained Permian age sandstone with a porosity of 17.5%, gas permeability of  $0.353 \mu\text{m}^2$  and no inclusions was selected for study in the experiments as a sedimentary rock. Prior to the experiments on nonstationary loading, sandstone samples with different diameters were prepared and tested on the Instron Series 4483 rig for uniaxial compressive strength in order to determine the zone of their linear elasticity. As a result, a sample with diameter  $d$  of 7.5 mm and length of 15.6 mm was selected as the one that could ensure that the dynamic experiment would be conducted in the zone of rock linear elasticity. Then, in order to study the dynamic Young's modulus depending on the loading frequency and amplitude, laboratory studies were performed on a small experimental set-up, shown in Figure 1 [21,22]. In the set-up, a rock sample was subjected to two types of loads: static preload  $F_{st}$  and dynamic load  $F_{dyn}$ . The static preload  $F_{st}$  was provided by a massive weight equaling 700 N. The dynamic load  $F_{dyn}$  (vibration) was provided by an Extrema 250  $\mu$  piezoelectric actuator powered with a sinusoidal signal from a MOS-01 CompactPower Titan series Manual generator (CA, USA). During the experiments, the amplitude  $A$  of the dynamic load  $F_{dyn}$  varied from 0 to 250 N; the loading frequency  $\omega$  varied from 15 to 40 Hz. The static weight and actuator were connected through a high adaptor. Experiments were conducted on nine samples, for which 270 experiments were carried out.

During the experiments, the instantaneous load data were provided by a Kistler 9027C load cell (Switzerland) mounted at the bottom of the set-up. The longitudinal displacement  $\Delta l$  of a sample's upper end surface was recorded by an eddy current probe (ECP) measuring the distance between itself and the low adaptor on top of a sample. The transverse displacement  $\Delta d/2$  of a sample's side surface was recorder by a Micro-epsilon optoNCDT 2300 laser sensor (Germany). Signals from the sensors were directed to a PC. The input signal data were acquired and synchronized in the interface developed in LabVIEW (TX, USA) and processed further in MATLAB (MA, USA). Measurements were conducted on 30 regimes (each regime was a combination of dynamic load frequency  $\omega$  and amplitude  $A$ ) and recorded by the interface for 3 seconds each.

During the experiments on nonstationary loading, the sample experienced cyclic nonlinear external force  $F$  that comprised static  $F_{st}$  and dynamic  $F_{dyn}$  parts (see Figure 2a). The maximum longitudinal deformation of a sample  $\Delta l$  was observed when the upper end surface of a sample was at the lowest position  $l_{min}$  from the ECP. Accordingly, the sample's length was  $l_{max}$  at the minimum external load. At the same time, at maximum external load, the sample's diameter was maximum,  $d_{max}$ , and at the minimum external load, the diameter was  $d_{min}$ . During the load cycle, a sample's side surface was displaced by  $\Delta d/2$ . The described rock deformation happened in the beginning of the zone of rock linear elasticity where stress  $\sigma$  and longitudinal strain  $\varepsilon_l$  are linked by a linear relationship and the Young's modulus  $E$  can be determined as  $E = d\sigma/d\varepsilon_l$  (see Figure 2b).

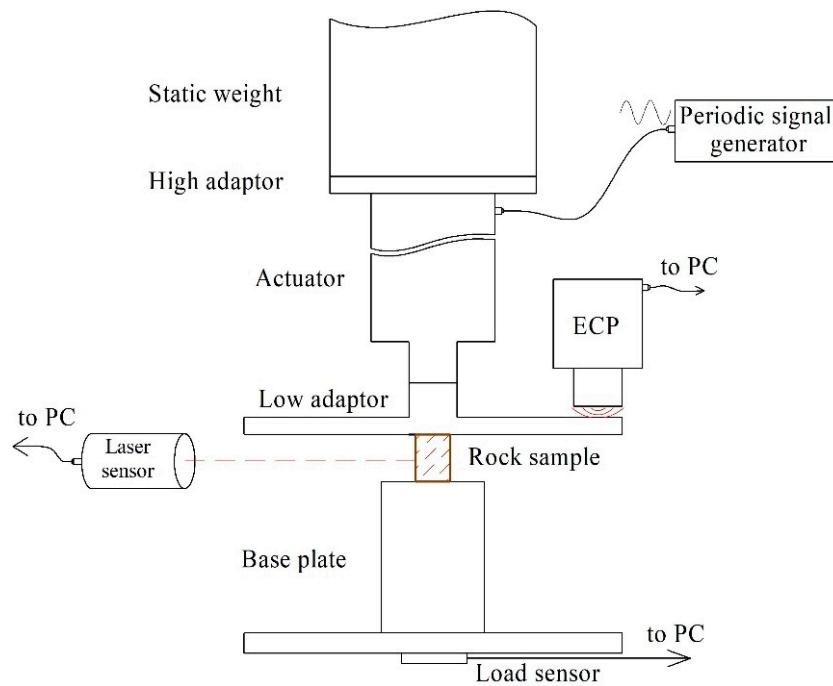


**Figure 1.** Schematics of the small experimental set-up: a rock sample was loaded with static load and dynamic load produced by an actuator that was powered with a periodic signal from a generator. External load was measured by a load sensor. The sample’s deformation was recorder by a laser sensor and an eddy current probe (ECP).

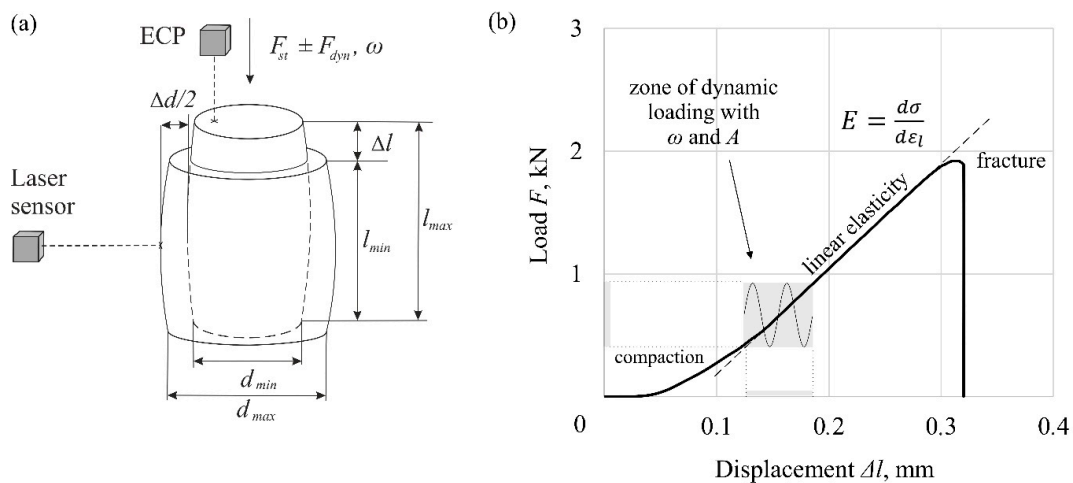


**Figure 2.** Experimental conditions: (a) schematics of rock sample deformation during the experiment; (b) stress state of a sample during dynamic loading.

The minimum  $l_{min}$  and maximum  $l_{max}$  sample lengths include static (determined by a static preload) and dynamic (determined by nonstationary load) components. Figure 3 shows that the sample length values  $l_{min}$  and  $l_{max}$  during vertical displacement of the sample’s upper end surface  $u = u(t)$  correspond to peak values of a dynamic load  $F_{dyn}$  spaced from each other in time by half an oscillation period,  $T/2$ , where  $T = 2\pi/\omega$ . The value  $l_0$  corresponds to a sample’s length in a preloaded state.

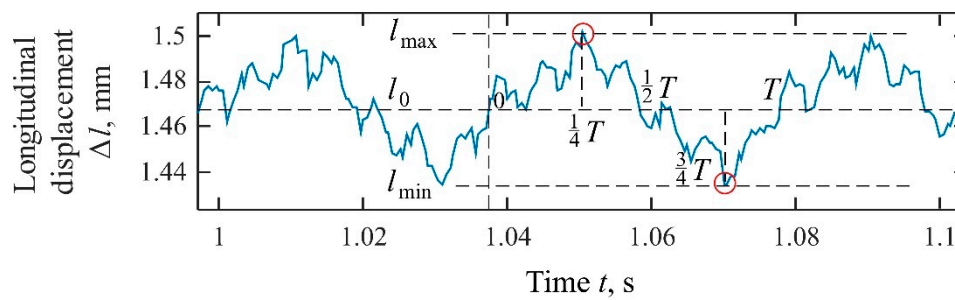


**Figure 3.** Longitudinal deformation of a sample in dynamic loading:  $F_{st} = 700$  N,  $A = 250$  N,  $\omega = 25$  Hz.

Since the stress  $\sigma$  and relative longitudinal strain  $\varepsilon_l$  of a sample are linked with a linear relationship (as shown in Figure 2b), the dynamic component of the Young's modulus,  $E_{dyn}$ , can be introduced by an analogy with the static Young's modulus and can be calculated using the following relations:

$$E_{dyn} = \frac{\Delta\sigma}{|\varepsilon_l|}, \Delta\sigma = \frac{2A}{S} |\varepsilon_l| = \frac{|\Delta l|}{l}, |\Delta l| = |l_{max} - l_{min}|, \quad (1)$$

where  $S$  refers to the cross-sectional area of a rock sample with a diameter of 7.5 mm.

Each calculated  $E_{dyn}$  value corresponds to a separate measurement at a particular regime defined by frequency  $\omega$  and amplitude  $A$ . The obtained calculated values of  $E_{dyn}$  for each particular regime were averaged over the nine rock samples studied. The results of  $E_{dyn}$  calculated using the relations in (1) are given in Figure 4.

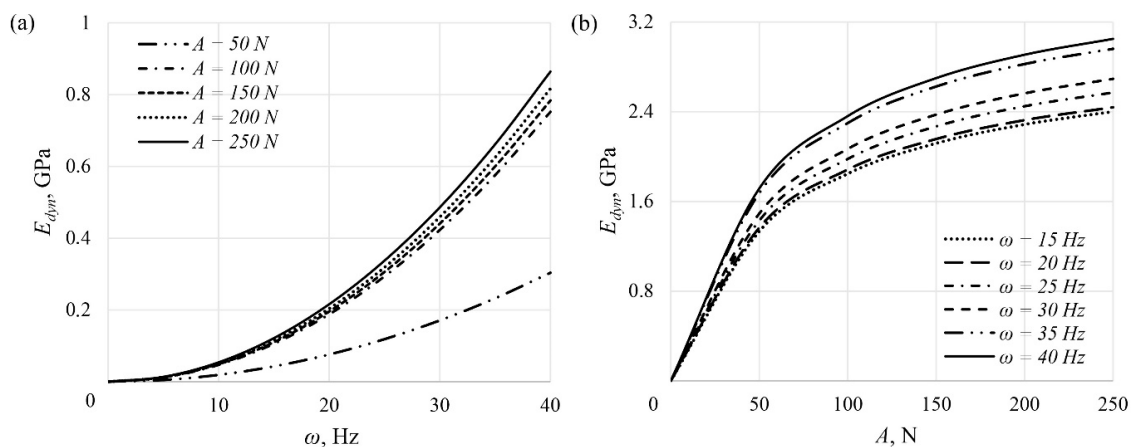


**Figure 4.** Experimental results on the dry sandstone dynamic Young's modulus  $E_{dyn}$ : (a) dependence of  $E_{dyn}$  on load frequency  $\omega$ ; (b) dependence of  $E_{dyn}$  on load amplitude  $A$ .

It can be seen from Figure 4 that  $E_{dyn}$  nonlinearly depends on the frequency  $\omega$  and amplitude  $A$  of the dynamic load, i.e.,  $E_{dyn} = E_{dyn}(\omega, A)$ . Such dispersion of the elastic modulus of a dry sedimentary rock needs to be properly considered in geotechnical engineering. Since at the moment there are no physical relations (models) in the literature able to capture the nonlinear behavior of the sandstone  $E_{dyn}$ , we propose one in the following section. As a conclusion of this section, let us highlight here that the nonlinear behavior of  $E_{dyn}$  in terms of the frequency  $\omega$  and amplitude  $A$ , obtained in the conducted experiments on nonstationary loading, forms the basis of the proposed developed model. In particular, the model should contain an  $\omega^2$  term, since Figure 4a shows a sort of quadratic relation between  $E_{dyn}$  and  $\omega$ .

### 3. Model Formulation

In general, modeling of rocks is usually performed within different approaches, such as multi-modular [23–25], block [26–29], hierarchy-block [30–33], and continuous medium [34–36]. In poromechanics, the dispersion of the elastic moduli of sedimentary rocks is considered by poroelastic models which describe the rock as a solid elastic matrix with infilling viscous fluid. Such models are intended to characterize in saturated porous media global inertia mechanisms [37], local “squirt” mechanisms [38–42], both global and local mechanisms [43], complex frequency-dependent macroscopic compressibility laws (double porosity model) [44], and significant compressional and shear dispersions (crack–spherical pore model) [45]. It is also known that in saturated sedimentary rocks, dispersion of the elastic moduli under high oscillating dynamic loads appears in undrained conditions [40].

The studies that we present in this paper are based on the results of experiments on a dry sandstone. Thus, there are no mechanisms that could lead to Young’s modulus dispersion connected to liquid viscosity. Among the experimental papers on dry sedimentary rocks, there are studies on elastic wave attenuation in Donnybrook sandstone in the frequency range from 0.1 Hz to 100 Hz [46] which at small strain ranging between  $10^{-8}$  and  $10^{-6}$  showed no dependence of the Young’s modulus on dynamic load frequency. Earlier studies of dry Navajo sandstone in the frequency range from 1 Hz to 4 kHz [47] also showed independence of rock elastic characteristics from the frequency of a dynamic load at small strain values of  $10^{-7}$ . Similarly, studies on dry Massillon, Berea, and Boise sandstones [48] in vacuum at frequencies up to 0.1 MHz did not reveal any relationship between attenuation and frequency at small strain, which is also relevant for man-made rocks with no intergranular cement.

It is known that the elastic moduli of granular sedimentary rocks depend on the rock loading path [2]. Provided that the loading is performed at high strain from the free state of a rock, the viscous and plastic mechanisms in a rock are related, as stated in [49–51], to structural effects (microcracks, viscous behavior of a rock matrix between cracks, and structural inertia forces). Such effects manifest on a stress–strain diagram as a hysteresis loop, which was observed, for example, in [52], during the study of dry Bandera sandstone at strain of  $10^{-3}$  until the rock was compacted. At the same time, the dynamic Young’s modulus exceeds the static one [53,54], and dispersion of the Young’s modulus with strain has been observed.

However, there have been no mentioned structural effects observed in the case when a rock sample experiences preloading. In a preloaded state the sample is compacted, i.e., its microcracks are closed and microstructures are in tight contact. A healed rock represents a solid medium in which viscous and plastic effects are blocked, and their association with dispersion of the elastic moduli is not observed.

The studies conducted in the present paper are based on the results of experiments in which a sandstone sample was initially stationarily preloaded and brought to linear elasticity when its microstructure was compacted and structural effects were not presented. Besides this, the strain of a sample was up to  $10^{-2}$  at dynamic load frequency of 40 Hz. In such conditions, in a sample there were only effects related to the acceleration of the load applied (axial inertial resistance of the rock to load). Consequently, the model of the dynamic Young’s modulus should consider only the inertial effects related to external nonstationary load.

The fact that in the series of experiments a static preload brought each sample into a state of linear elasticity allows us to use the idealized model of the system proposed in Chapter 6 “Laboratory testing of rocks” of reference [55]. Similarly, a rock sample is considered as a spring with stiffness  $k$ , the lower point  $O$  of which is fixed, and the upper point  $A$  carries a mass  $m$  (as shown in Figure 5). A sample experiences force  $F_{dyn}$ , determined by an external dynamic load, and force  $F_e$  generated by the elastic energy of the rock matrix.



**Figure 5.** The “mass-on-a-spring” model: (a) a sample in the set-up; (b) schematics of the model.

The displacement of a mass  $u = u(t)$  from an equilibrium position specifies changes in a sample’s length, which allows us to calculate  $l_{min}$  and  $l_{max}$  in (1). In accordance with Newton’s second law, the Equation for mass is determined by the relation

$$m\ddot{u} = F_{dyn} + F_e - mg, \quad (2)$$

in which the last term takes into account the gravitational force. The order of magnitude of the sample’s mass is  $m \sim 10^{-3}$  kg; therefore,  $mg \sim 10^{-2}H$ . Since  $|F_{dyn}| \sim |F_e| \sim 10^2 \text{ N} \gg mg$ , the influence of the gravitational force on the dynamics of the mass in (2) can be neglected. Considering that the elastic force  $F_e = -ku$ , and the loading on the sample was carried out according to the law  $F_{dyn} = A \sin \omega t$ , Equation (2) can be rewritten as

$$m\ddot{u} = A \sin \omega t - ku. \quad (3)$$

Thus, the description of a rock sample’s upper end motion is mathematically reduced to studying the dynamics of mass  $m$  on a spring. Within the framework of this model, the displacement of all points of a sample occurs according to the same law, regardless of the location of the selected point in a sample.

It is well known from [56] that the general solution of the Equation of motion (3) consists of the general solution of the homogeneous Equation (free oscillation) plus the particular solution of the inhomogeneous Equation:

$$u(t) = C \sin \Omega t + B \sin \omega t, \quad (4)$$

where  $C \sin \Omega t$  represents the elastic response of a sample and  $B \sin \omega t$  expresses the response of a sample under  $F_{dyn}$ ;  $B, C$  are vibration amplitudes;  $\Omega$  is the natural frequency. Substituting (4) into (3) and after differentiation, by equating the respective coefficients of  $\sin \Omega t$  and  $\sin \omega t$ , we obtain

$$\Omega^2 = \frac{k}{m}, B = \frac{A}{k - \omega^2 m} = \frac{A}{m(\Omega^2 - \omega^2)}. \quad (5)$$

The maximum extension of the specimen under dynamic loading is calculated for  $t = T/4 = \pi/2\omega$  and is equal to

$$l_{max} = l_0 + u(T/4) = B + C \sin \frac{\pi \Omega}{2 \omega}. \quad (6)$$

The minimum extension of the specimen is calculated for  $t = 3T/4 = 3\pi/2\omega$ :

$$l_{min} = l_0 + u(3T/2) = -B + C \sin \left( \frac{3\pi \Omega}{2 \omega} \right). \quad (7)$$

Then, from (6) and (7) we obtain

$$\Delta l = l_{max} - l_{min} = 2B - 2C \sin \left( \frac{\pi \Omega}{2 \omega} \right) \cos \left( \frac{\pi \Omega}{\omega} \right), \quad (8)$$

where we used reference formulas for adding the trigonometric functions.

We assume that the natural rock matrix frequency of oscillations  $\Omega$  is linked with the frequency of disturbing oscillations  $\omega$  via some function  $\Omega = \alpha\omega$ , where coefficient  $\alpha \gg 1$  means that the intrinsic matrix oscillation surpasses the external load oscillation. The coefficient  $B$  is determined from (5); then (8) can be represented as

$$|\Delta l| = \left| \frac{2A}{m[\alpha^2 - 1]\omega^2} - 2C \sin \frac{\pi\alpha}{2} \cos \pi\alpha \right|. \quad (9)$$

From here and from (1) follows the formula for the dynamic component of the Young's modulus:

$$E_{dyn} = \frac{A}{\frac{S}{l} \left| \frac{A}{m[\alpha^2 - 1]\omega^2} - C \sin \frac{\pi\alpha}{2} \cos \pi\alpha \right|}. \quad (10)$$

Parameters  $C$ ,  $\Omega$ ,  $\omega$ , and  $m$  were selected based on the analysis of experimental data.

#### 4. Results and Discussion

The developed model (10) was applied to the experimental conditions (input parameters), such as the physical parameters of a studied sample (diameter  $d$ , length  $l$ , and mass  $m$ ) and parameters characterizing the loading regime (frequency  $\omega$  and amplitude  $A$  of the nonstationary dynamic load  $F_{dyn}$ ), and the dynamic Young's modulus  $E_{dyn \text{ model}}$  was obtained. As a result of calculation, in a 3D space, formula (10) defined the surface shown in Figure 6.

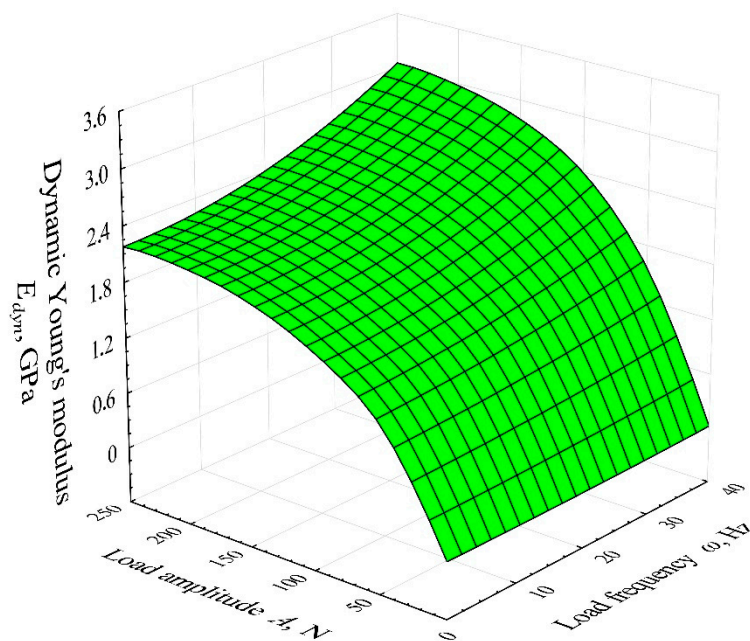


**Figure 6.** The modelled nonlinear nature of the dynamic Young's modulus,  $E_{dyn \text{ model}}$ , depending on the frequency  $\omega$  and amplitude  $A$  of nonstationary load.

Since it is necessary to consider the intrinsic sedimentary rock matrix oscillation  $\Omega$ , model (10) contains the parameter  $\alpha$ , which depends on the rock microstructure and represents the ratio of the frequencies of natural and external  $\omega$  oscillations. Analysis of the laboratory experimental results gave the value  $\alpha \approx 5 \times 10^4$ . The parameter  $C$  in the model represents the reaction of the rock sample to a combination of all other mentioned parameters (conditions). In fact, if we express  $C$  from (10) and substitute the units of measurement for all model parameters according to the international system of quantities, then for a set of experimental data,  $C$  takes values in range from  $2 \times 10^{-5}$  to  $5 \times 10^{-5} \left\{ \frac{m}{s^2 \text{Hz}^2} - \text{kg} \times m \right\}$ . Both parameters  $\alpha$  and  $C$  were found during model adjustment while

comparing laboratory experimental results on the dynamic Young’s modulus  $E_{dyn}$  with the obtained  $E_{dyn\ model}$  values.

In accordance with Figure 6, and considering (10), the dynamic Young’s modulus  $E_{dyn\ model}$  in 2D space can roughly be described through the frequency  $\omega$  of the applied dynamic load using a quadratic function with constants  $G$  and  $H$  of the kind

$$E_{dyn\ model}(\omega) = G\omega^2 + H, \tag{11}$$

where  $H = 0$ , since at  $\omega = 0$ , we have  $E_{dyn} = 0$ . Herein, the higher the load amplitude  $A$ , the higher the  $G$  and  $F_{dyn}$  gradient.

In order to estimate the accuracy of model (10) using (11) for each amplitude  $A$  of an applied dynamic load  $F_{dyn}$ , the following Equations were obtained:

$$\begin{aligned} E_{dyn\ 50\ N} &= 1.85 \times 10^{-4} \omega^2, \\ E_{dyn\ 100\ N} &= 4.54 \times 10^{-4} \omega^2, \\ E_{dyn\ 150\ N} &= 4.69 \times 10^{-4} \omega^2, \\ E_{dyn\ 200\ N} &= 5.20 \times 10^{-4} \omega^2, \\ E_{dyn\ 250\ N} &= 5.80 \times 10^{-4} \omega^2. \end{aligned} \tag{12}$$

The accuracy of the model was evaluated for each dynamic load amplitude  $A$  through the scheme described hereafter. Amplitudes of 15, 25, and 35 Hz were selected by alternation. For the selected amplitudes, using model values of the dynamic Young’s modulus,  $E_{dyn\ model}$ , for all the samples, an approximation function (second-order polynomial) was built. Then, with the help of the approximating function, the values of  $E_{dyn\ calc}$  were interpolated for frequencies 20, 30, and 40 Hz (as shown in Figure 7). The obtained interpolated values of  $E_{dyn\ calc}$  were compared with the initial values of  $E_{dyn\ model}$  gathered by the model (10); the deviation  $R$  was calculated by the formula

$$R = \frac{E_{dyn\ calc} - E_{dyn\ model}}{E_{dyn\ model}} \times 100 \%. \tag{13}$$

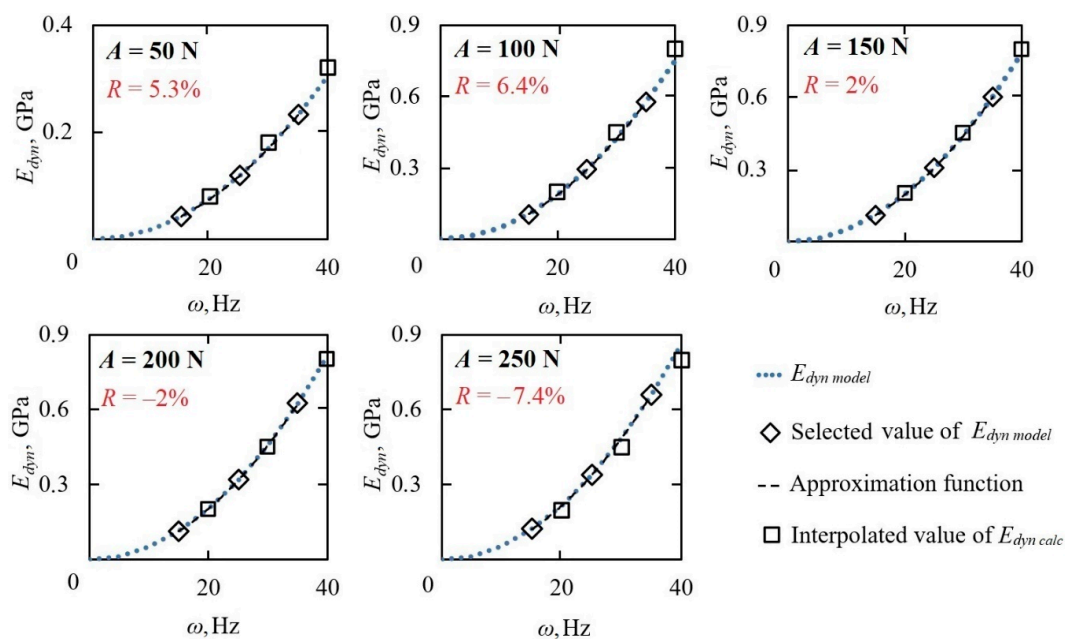


Figure 7. Model examination.

It was found that the developed mathematical model was characterized by high accuracy. Using the developed model allows us to avoid error when calculating the dynamic Young's modulus  $E_{dyn}$ , which can reach values ranging from  $-7.4\%$  to  $6.4\%$ .

The obtained mathematical model reflects the real nature of the dynamic Young's modulus  $E_{dyn}$  approved by experimental data. The relations underlying the model can be used as a basis for further explanation of the phenomenon of dispersion of the Young's modulus of sedimentary rocks under the influence of nonstationary load with frequency  $\omega$  and amplitude  $A$ .

It has to be stated that the dynamic component of the Young's modulus of a dry sedimentary rock, such as sandstone, had not been previously modelled. In comparison with other techniques for evaluating the dynamic Young's modulus, the proposed model reflects the nonlinear behavior of the dynamic component of the Young's modulus and calculates it. This is possible because there are physically substantiated relations forming the basis of the model. Since the model is built on the principles of classical mechanics, the model is simple and reliable in the dynamic load frequency range from 15 to 40 Hz and amplitude range from 50 to 250 N. In these conditions, the model shows the dispersion of the dynamic Young's modulus with load frequency and amplitude. The model allows us to obtain in 3D a spatial passport (see Figure 6) of the nonlinear dynamic component of the Young's modulus subjected to nonstationary loading. This passport allows us to forecast the value of the dynamic Young's modulus in the given range of load frequency and amplitude.

Obtained in experiments, the laboratory results revealed a nonlinear increase in the dynamic Young's modulus with load frequency and amplitude. Accordingly, a hypothesis of nonlinear dependence of the dynamic Young's modulus on nonstationary load frequency and amplitude formed the foundation of the model. With the help of rigorous physically substantiated mechanical relations and mathematical techniques, the model was derived and formulated. Then the model was applied to the experimental conditions (input parameters), after which it was adjusted, and the model matched the laboratory results. The model was examined at five amplitudes, and its reliability was proved. This novel mathematical model reflects the nonlinear nature of the dynamic Young's modulus depending on nonstationary load frequency and amplitude.

## 5. Conclusions

In this work, we presented a mathematical model of the dynamic Young's modulus of a dry sedimentary rock subjected to nonstationary loading. The model was built based on common concepts of rock mechanics using physical parameters of the sandstone samples, including their dimensions and mass. It considers both external disturbing load frequency and internal natural rock matrix oscillations via parameter  $\alpha$  which is determined by the rock microstructure. Each particular combination of experimental parameters is considered in the model by parameter  $C$ . Using the initial experimental conditions, the developed model in 3D space built a dynamic Young's modulus surface defined by the frequency and amplitude of a dynamic load, and it matched the experimental data. Characterizing 2D functions of the Young's modulus in terms of frequency allowed us to confirm the model's reliability.

Based on the study undertaken, the nonlinear nature of the dynamic Young's modulus of sedimentary rock such as dry sandstone under nonstationary loading with increasing frequency and amplitude of the load can be captured with the novel developed mathematical model.

**Author Contributions:** M.G. proposed the approach and described the model; E.R. performed model adjustment; M.T. examined the model; E.K. prepared drawings; V.P. prepared the initial data. All authors have read and agreed to the published version of the manuscript.

**Funding:** The support of the Russian Science Foundation (Project No. 19-19-00408) is gratefully acknowledged.

**Conflicts of Interest:** The authors are aware of their ethical responsibilities and they declare that they have no conflicts of interest.

## List of Symbols

$A$	Amplitude of the dynamic load, N
$d_{max}$	Maximum value of sample's diameter, m
$d_{min}$	Minimum value of sample's diameter, m
$E_{dym\ calc}$	Calculated dynamic component of the Young's modulus, Pa
$E_{dym\ model}$	Model dynamic component of the Young's modulus, Pa
$E_{dym}$	Dynamic component of the Young's modulus, Pa
$F_{st}$	Static preload, N
$g$	Gravity, $m/s^2$
$k$	Stiffness
$l$	Sample length, m
$l_0$	Sample length in the preloaded state, m
$l_{max}$	Maximum sample length, m
$l_{min}$	Minimum sample length, m
$m$	Mass, m
$R$	Percentage deviation
$S$	Cross-section area of the sample, $m^2$
$T$	Period, s
$t$	Time, s
$u$	Displacement, m
$u_{max}$	Maximum displacement, m
$u_{min}$	Minimum displacement, m
$\alpha$	Coefficient linking external and natural frequencies
$\Delta d$	Transverse displacement, m
$\Delta l$	Longitudinal displacements, m
$\varepsilon_l$	Longitudinal strain
$\pi$	Ratio of a circle's circumference to its diameter
$\sigma$	Stress, Pa
$\omega$	External frequency, Hz
$\Omega$	Natural frequency, Hz

## References

1. Muir, T.G.; Cormack, J.M.; Slack, C.M.; Hamilton, M.F. Elastic softening of sandstone due to a wideband acoustic pulse. *J. Acoust. Soc. Am.* **2020**, *147*, 1006–1014. [[CrossRef](#)] [[PubMed](#)]
2. Peng, K.; Zhou, J.; Zou, Q.; Song, X. Effect of loading frequency on the deformation behaviours of sandstones subjected to cyclic loads and its underlying mechanism. *Int. J. Fatigue* **2020**, *131*, 105349. [[CrossRef](#)]
3. Rivière, J.; Shokouhi, P.; Guyer, R.A.; Johnson, P.A. A set of measures for the systematic classification of the nonlinear elastic behavior of disparate rocks. *J. Geophys. Res. Solid Earth* **2015**, *120*, 1587–1604. [[CrossRef](#)]
4. Lozovyi, S.; Bauer, A. Static and dynamic stiffness measurements with Opalinus Clay. *Geophys. Prospect.* **2019**, *67*, 997–1019. [[CrossRef](#)]
5. Yin, S.; Xie, R. Experimental analysis of dynamic and static mechanical properties of deep thick anhydrite cap rocks under high-stress conditions. *Carbonates Evaporites* **2018**, *34*, 807–823. [[CrossRef](#)]
6. Sone, H.; Zoback, M.D. Mechanical properties of shale-gas reservoir rocks—Part 1: Static and dynamic elastic properties and anisotropy. *Geophysics* **2013**, *78*, D381–D392. [[CrossRef](#)]
7. Wang, Y.; Zhao, L.; Han, D.-H.; Qin, X.; Ren, J.; Wei, Q. Micro-mechanical analysis of the effects of stress cycles on the dynamic and static mechanical properties of sandstone. *Int. J. Rock Mech. Min. Sci.* **2020**, *134*, 104431. [[CrossRef](#)]
8. Petrie, E.S.; Jeppson, T.N.; Evans, J.P. Predicting rock strength variability across stratigraphic interfaces in caprock lithologies at depth: Correlation between outcrop and subsurface. *Environ. Geosci.* **2012**, *19*, 125–142. [[CrossRef](#)]
9. Nazari Ostad, M.; Niri, M.E.; Darjani, M. 3D modeling of geomechanical elastic properties in a carbonate-sandstone reservoir: A comparative study of geostatistical co-simulation methods. *J. Geophys. Eng.* **2018**, *15*, 1419–1431. [[CrossRef](#)]

10. Zuo, J.-P.; Wei, X.; Shi, Y.; Liu, C.; Li, M.; Wong, R.H.C. Experimental study of the ultrasonic and mechanical properties of a naturally fractured limestone. *Int. J. Rock Mech. Min. Sci.* **2020**, *125*, 104162. [[CrossRef](#)]
11. Li, X.B.; Lok, T.S.; Zhao, J. Dynamic characteristics of granite subjected to intermediate loading rate. *Rock Mech. Rock Eng.* **2005**, *38*, 21–39. [[CrossRef](#)]
12. Szewczyk, D.; Bauer, A.; Holt, R.M. A new laboratory apparatus for the measurement of seismic dispersion under deviatoric stress conditions. *Geophys. Prospect.* **2016**, *64*, 789–798. [[CrossRef](#)]
13. Szewczyk, D.; Holt, R.M.; Bauer, A. The impact of saturation on seismic dispersion in shales—laboratory measurements. *Geophysics* **2018**, *83*, 15–34. [[CrossRef](#)]
14. Batzle, M.L.; Han, D.-H.; Hofmann, R. Fluid mobility and frequency-dependent seismic velocity—Direct measurements. *Geophysics* **2006**, *71*, N1–N9. [[CrossRef](#)]
15. Pimienta, L.; Fortin, J.; Guéguen, Y. Bulk modulus dispersion and attenuation in sandstones. *Geophysics* **2015**, *80*, A25–A30. [[CrossRef](#)]
16. Gong, F.; Di, B.; Wei, J.; Ding, P.; Tian, H.; Han, J. A study of the anisotropic static and dynamic elastic properties of transversely isotropic rocks. *Geophysics* **2019**, *84*, C281–C293. [[CrossRef](#)]
17. Bagde, M.N.; Petroš, V. Fatigue properties of intact sandstone samples subjected to dynamic uniaxial cyclical loading. *Int. J. Rock Mech. Min. Sci.* **2005**, *42*, 237–250. [[CrossRef](#)]
18. Aghaei Araei, A.; Razeghi, H.R.; Ghalandarzadeh, A.; Hashemi Tabatabaei, S. Effects of loading rate and initial stress state on stress-strain behavior of rock fill materials under monotonic and cyclic loading conditions. *Sci. Iran.* **2012**, *19*, 1220–1235. [[CrossRef](#)]
19. Zhang, Z.; Wang, T.; Wu, S.; Tang, H.; Xin, P.; Liang, C. Dynamics stress–strain behavior of Tianshui soils. *Landslides* **2017**, *14*, 323–335. [[CrossRef](#)]
20. ASTM Standard D3999-91. Standard D3999-91. Standard test methods for the determination of the modulus and damping properties of soils using the cyclic triaxial apparatus. In *Annual Book of ASTM Standard*; ASTM International: West Conshohocken, PA, USA, 2003.
21. Riabokon, E.P. Laboratory study on the effect of elastic wave treatment on geomechanical and capillary properties of clastic reservoirs. *Neftyanoe Khozyaystvo—Oil Ind.* **2020**, *4*, 54–57. [[CrossRef](#)]
22. Wiercigroch, M.; Riabokon, E.P.; Guzev, M.A.; Turbakov, M.S.; Kobiakov, D.V. Experimental studies on static and dynamic loading of heterogeneous rocks. In Proceedings of the XLVIII International Conference Advanced Problems in Mechanics, Saint Petersburg, Russia, 21–26 June 2020; p. 55.
23. Lomakin, E.V. Mechanics of media with stress-state dependent properties. *Phys. Mesomech.* **2007**, *10*, 255–264. [[CrossRef](#)]
24. Myasnikov, V.P.; Sadovskii, V.M. Variational principles of the theory of the limiting equilibrium of media with different strengths. *J. Appl. Math. Mech.* **2004**, *68*, 437–446. [[CrossRef](#)]
25. Min, K.-B.; Jing, L. Stress dependent mechanical properties and bounds of Poisson’s ratio for fractured rock masses investigated by a DFN-DEM technique. *Int. J. Rock Mech. Min. Sci.* **2004**, *41*, 1–6. [[CrossRef](#)]
26. Makarov, P.V. Evolutionary nature of structure formation in lithospheric material: Universal principle for fractality of solids. *Russ. Geol. Geophys.* **2007**, *48*, 558–574. [[CrossRef](#)]
27. Grayeli, R.; Mortazavi, A. Discontinuous deformation analysis with second-order finite element meshed block. *Int. J. Numer. Anal. Methods Geomech.* **2006**, *30*, 1545–1561. [[CrossRef](#)]
28. Sadovskii, V.M.; Sadovskaya, O.V. Supercomputer modeling of wave propagation in blocky media accounting fractures of interlayers. *Adv. Struct. Mater.* **2020**, *122*, 379–398. [[CrossRef](#)]
29. Liu, G.-Y.; Xu, W.-J.; Govender, N.; Wilke, D.N. A cohesive fracture model for discrete element method based on polyhedral blocks. *Powder Technol.* **2020**, *359*, 190–204. [[CrossRef](#)]
30. Chanyshv, A.I.; Belousova, O.E. A method to describe hierarchical block structure of rock mass, considering nonuniformity of mechanical properties. *J. Min. Sci.* **2017**, *53*, 441–448. [[CrossRef](#)]
31. Wang, W.; Chen, S. 3D elasto-visco-plastic hierarchical block element method for rock mass. *Yanshilixue Yu Gongcheng Xuebao/Chin. J. Rock Mech. Eng.* **2003**, *22*, 525–531.
32. Li, J.; Chen, W.; Shi, C.; Wang, M. Calculation method of irreversible displacement region radius based on block hierarchical structure under large-scale underground explosion. *Baozha Yu Chongji/Explos. Shock Waves* **2018**, *38*, 1271–1277. [[CrossRef](#)]
33. Oparin, V.N.; Tanaino, A.S. Canonical ranking of sizes of structural units in rocks classifications. *J. Min. Sci.* **2009**, *45*, 551–562. [[CrossRef](#)]

34. Nikafshan Rad, H.; Jalali, Z.; Jalalifar, H. Prediction of rock mass rating system based on continuous functions using Chaos-ANFIS model. *Int. J. Rock Mech. Min. Sci.* **2015**, *73*, 1–9. [[CrossRef](#)]
35. Müller, L. *Rock Mechanics*; Springer: Wien, Austria; New York, NY, USA, 1982.
36. Brocato, M. A continuum model of close packing granular materials for the study of rock filled gabions. *Int. J. Solids Struct.* **2020**, *187*, 38–47. [[CrossRef](#)]
37. Biot, M.A. Theory of propagation of elastic waves in a fluid-saturated porous solid II. Higher frequency range. *J. Acoust. Soc. Am.* **1956**, *28*, 179–191. [[CrossRef](#)]
38. O'Connell, R.J.; Budiansky, B. Viscoelastic properties of fluid-saturated cracked solids. *J. Geophys. Res.* **1977**, *82*, 5719–5735. [[CrossRef](#)]
39. Mavko, G.; Nur, A. Melt squirt in the asthenosphere. *J. Geophys. Res.* **1975**, *80*, 1444–1448. [[CrossRef](#)]
40. Murphy, W.F., III; Winkler, K.W.; Kleinberg, R.L. Acoustic relaxation in sedimentary rocks: Dependence on grain contacts and fluid saturation. *Geophysics* **1986**, *51*, 757–766. [[CrossRef](#)]
41. Johnston, D.H.; Toksoz, M.N.; Timur, A. Attenuation of seismic waves in dry and saturated rocks—II. Mechanisms. *Geophysics* **1979**, *44*, 691–711. [[CrossRef](#)]
42. Endres, A.L.; Knight, R.J. Incorporating pore geometry and fluid pressure communication into modeling the elastic behavior of porous rocks. *Geophysics* **1997**, *62*, 106–115. [[CrossRef](#)]
43. Dvorkin, J.; Nur, A. Dynamic poroelasticity: A unified model with the squirt and the Biot mechanisms. *Geophysics* **1993**, *58*, 524–533. [[CrossRef](#)]
44. Pride, S.R.; Berryman, J.G. Linear dynamics of double-porosity dual-permeability materials. I. Governing equations and acoustic attenuation. *Phys. Rev. E Stat. Nonlinear Soft Matter Phys.* **2003**, *68*, 366031–3660310. [[CrossRef](#)] [[PubMed](#)]
45. Chapman, M.; Zatsepin, S.V.; Crampin, S. Derivation of a microstructural poroelastic model. *Geophys. J. Int.* **2002**, *151*, 427–451. [[CrossRef](#)]
46. Mikhaltsevitch, V.; Lebedev, M.; Gurevich, B. A laboratory study of the elastic and anelastic properties of the sandstone flooded with supercritical CO<sub>2</sub> at seismic frequencies. *Energy Procedia* **2014**, *63*, 4289–4296. [[CrossRef](#)]
47. Spencer, J.W., Jr. Stress relaxations at low frequencies in fluid-saturated rocks: Attenuation and modulus dispersion. *J. Geophys. Res.* **1981**, *86*, 1803–1812. [[CrossRef](#)]
48. Winkler, K.W. Frequency dependent ultrasonic properties of high-porosity sandstones. *J. Geophys. Res.* **1983**, *88*, 9493–9499. [[CrossRef](#)]
49. Zhang, Q.B.; Zhao, J. A review of dynamic experimental techniques and mechanical behaviour of rock materials. *Rock Mech. Rock Eng.* **2014**, *47*, 1411–1478. [[CrossRef](#)]
50. Ožbolt, J.; Sharma, A.; Reinhardt, H.-W. Dynamic fracture of concrete—Compact tension specimen. *Int. J. Solids Struct.* **2011**, *48*, 1534–1543. [[CrossRef](#)]
51. Bažant, Z.P.; Shang-Ping, B.; Ravindra, G. Fracture of rock: Effect of loading rate. *Eng. Fract. Mech.* **1993**, *45*, 393–398. [[CrossRef](#)]
52. Tutuncu, A.N.; Podio, A.L.; Gregory, A.R.; Sharma, M.M. Nonlinear viscoelastic behavior of sedimentary rocks, Part I: Effect of frequency and strain amplitude. *Geophysics* **1998**, *63*, 184–194. [[CrossRef](#)]
53. Saksala, T. On the strain rate sensitivity of coarse-grained rock: A mesoscopic numerical study. *Rock Mech. Rock Eng.* **2019**, *52*, 3229–3240. [[CrossRef](#)]
54. Denoual, C.; Hild, F. A damage model for the dynamic fragmentation of brittle solids. *Comput. Methods Appl. Mech. Eng.* **2000**, *183*, 247–258. [[CrossRef](#)]
55. Jaeger, J.C.; Cook, N.G.W.; Zimmerman, R.W. Laboratory testing of rocks. In *Fundamentals of Rock Mechanics*, 4th ed.; Blackwell Publishing: Malden, MA, USA, 2007; pp. 145–167.
56. Goldstein, H.; Poole, C., Jr.; Safko, J. *Classic Mechanics*, 3rd ed.; Addison Wesley: San Francisco, CA, USA, 2002.

**Publisher's Note:** MDPI stays neutral with regard to jurisdictional claims in published maps and institutional affiliations.



© 2020 by the authors. Licensee MDPI, Basel, Switzerland. This article is an open access article distributed under the terms and conditions of the Creative Commons Attribution (CC BY) license (<http://creativecommons.org/licenses/by/4.0/>).